Video Article

Atomic Force Microscopy Investigations of DNA Lesion Recognition in Nucleotide Excision Repair

Jonas Gross*[1], Nicolas Wirth*[1], Ingrid Tessmer[1]

[1]Rudolf Virchow Center for Experimental Biomedicine, University of Würzburg

*These authors contributed equally

Correspondence to: Ingrid Tessmer at Ingrid.Tessmer@virchow.uni-wuerzburg.de

URL: https://www.jove.com/video/55501
DOI: doi:10.3791/55501

Keywords: Genetics, Issue 123, Atomic force microscopy (AFM), protein-DNA interaction, DNA repair, nucleotide excision repair (NER), DNA lesion recognition, DNA modification, AFM sample preparation, AFM volume analysis, DNA binding position analysis.

Date Published: 5/24/2017

Citation: Gross, J., Wirth, N., Tessmer, I. Atomic Force Microscopy Investigations of DNA Lesion Recognition in Nucleotide Excision Repair. *J. Vis. Exp.* (123), e55501, doi:10.3791/55501 (2017).

Abstract

AFM imaging is a powerful technique for the study of protein-DNA interactions. This single molecule method allows the simultaneous resolution of different molecules and molecular assemblies in a heterogeneous sample. In the particular context of DNA interacting protein systems, different protein complex forms and their corresponding binding positions on target sites containing DNA fragments can thus be distinguished. Here, an application of AFM to the study of DNA lesion recognition in the prokaryotic and eukaryotic nucleotide excision DNA repair (NER) systems is presented. The procedures of DNA and protein sample preparations are described and experimental as well as analytical details of the experiments are provided. The data allow important conclusions on the strategies by which target site verification may be achieved by the NER proteins. Interestingly, they indicate different approaches of lesion recognition and identification for the eukaryotic NER system, depending on the type of lesion. Furthermore, distinct structural properties of the two different helicases involved in prokaryotic and eukaryotic NER result in and explain the different strategies observed for these two systems. Importantly, these experimental and analytical approaches can be applied not only to the study of DNA repair but also very similarly to other DNA interacting protein systems such as those involved in replication or transcription processes.

Video Link

The video component of this article can be found at https://www.jove.com/video/55501/

Introduction

Atomic force microscopy (AFM) is a powerful technique for the analysis of protein-DNA interactions[1,2,3,4,5,6,7,8,9]. It requires only low amounts of sample material to directly visualize heterogeneous samples with a resolution at the single molecule level. Heterogeneity can result from different conformational or oligomeric states of a protein. In particular, in the context of protein-DNA samples, protein complexes can display different stoichiometries and/or conformations induced by DNA binding in general or binding to a specific target site within DNA. Heterogeneous samples may also contain two (or more) different kinds of proteins, and different protein complex forms (*e.g.*, consisting of only one type of protein versus heteromeric complexes) may interact differently with DNA. The studies discussed here exploit AFM imaging in air on static, dried samples of DNA repair proteins bound to long (~900 base pairs, bp) DNA fragments that contain a lesion, which represents a target of these proteins. The high, molecular resolution of AFM allows the distinction between different types of protein complexes and to determine the binding positions of the proteins on the DNA fragments. Importantly, the lesions are introduced into the DNA substrates at well-defined positions. Because the position of the lesion site in the DNA is known, the distributions of proteins bound on DNA provide insight into (different) lesion recognition properties of the (different) protein complexes, *e.g.*, how well they recognize a particular type of lesion (compared to non-damaged DNA)[2,3,4,5,6]. Their positions on the DNA also allow the distinction between protein complexes bound specifically at the lesions and complexes bound nonspecifically elsewhere on the DNA. Separate characterization of these different complex types (complexes bound specifically at the lesion versus nonspecific complexes) can reveal potential conformational changes in the complexes induced upon target site identification.

The DNA repair proteins focused on here are helicases that are responsible for lesion recognition in the nucleotide excision repair (NER) pathway. In bacteria, NER is achieved by the proteins UvrA, UvrB, and UvrC. UvrA is responsible for initial lesion sensing in a $UvaA_2$/$UvrB_2$ DNA-scanning complex. Upon lesion verification by UvrB this complex converts to monomeric UvrB bound at the lesion site and this specific complex can then recruit the prokaryotic NER endonuclease UvrC. UvrC excises a short (12-13 nt) stretch of single stranded DNA (ssDNA) containing the lesion. The missing stretch is then refilled by DNA polymerase. Finally, DNA ligase seals the newly synthesized stretch with the original DNA[9,10]. In eukaryotes, most proteins of the NER cascade are part of the large, multimeric transcription factor II H (TFIIH) complex. After initial lesion sensing *via* the trimeric CEN2-XPC-HR23B complex, TFIIH is recruited to the DNA target site. When XPD within the complex verifies the presence of an NER target lesion, the eukaryotic NER endonucleases XPG and XPF are recruited to excise a short (24-32 nt) stretch of ssDNA containing the lesion[9,10]. Here, specifically, the helicases UvrB and XPD from prokaryotic and eukaryotic NER, respectively, were studied. These helicases require an unpaired region in the DNA (a DNA bubble) to thread onto one of the two DNA single strands and subsequently translocate

Copyright © 2017 Journal of Visualized Experiments

along this strand fueled by ATP hydrolysis. In addition to the DNA lesions, a DNA bubble was hence introduced in the substrates that functions as loading site for the proteins.

The procedure for preparation of specific lesion DNA substrates has been described previously[11]. It requires a circular DNA construct (plasmid) with two closely spaced restriction sites for a nickase. In the context of this study, the plasmid pUC19N (2729 bp) was used (created by S. Wilson's laboratory, NIEHS). This plasmid contains three closely spaced restriction sites for the nickase Nt.BstNBI that frame a 48 nucleotide (nt) stretch. After incubation with the nickase, the stretch of ssDNA between these sites can be removed and replaced by an oligonucleotide containing any target feature. After each step, complete enzymatic digestion is tested via agarose gel electrophoresis. Nicked circular DNA can be distinguished due to its lower electrophoretic mobility compared to the original supercoiled plasmid. Gapping of the DNA and replacement of the removed stretch by the specific substrate oligonucleotide can be evaluated via digestion with a restriction enzyme which incises the substrate exclusively within the region between the nicks. Linearization of the circular plasmid by the enzyme will hence be suppressed for the gapped DNA and restored after insertion of the specific oligonucleotide. Finally, two endonuclease restriction sites (ideally single cutters) allow for the generation of a linear DNA substrate, with length as desired and with the specific target site at a defined position as well as a DNA bubble at a distance from the lesion either in 5' or 3' direction.

Recognition of the lesions by the NER helicases can be investigated *via* AFM imaging. Stalled DNA translocation of the helicases at the lesion site is visible as a peak in the protein position distribution on the DNA and indicates lesion recognition. Because DNA translocation of these helicases is furthermore directional, with 5'-to-3' polarity, the dependence of lesion recognition on the position of the loading site (DNA bubble upstream or downstream from the lesion) also indicates whether the lesion is preferentially recognized on the translocated or on the opposite, non-translocated ssDNA strand[5,9]. In the following sections, the methods used will be introduced and major findings from these experiments will be briefly discussed. Importantly, analogous to the exemplary work on DNA repair shown here, AFM imaging can be applied to the study of different DNA interacting systems, such as DNA replication or transcription[8,12,13,14].

Protocol

1. Sample Preparation

1. **Preparation of DNA substrates**[11]
    1. Generating a ssDNA gap in the plasmid
        1. Completely digest a sample of the plasmid (here: modified pUC19, pUC19N) in a reaction tube with an appropriate nickase (here: Nt.BstNBI) followed by enzyme heat inactivation, using conditions according to the manufacturer's protocol (see Figure 1 for a schematic presentation). Start with ~50 µL and ~500 nM plasmid for a sufficient yield.
        2. Verify plasmid nicking by agarose gel electrophoresis on diluted samples (~20 nM)[15]. Wear gloves for protection against the DNA binding dye used for DNA visualization.
        NOTE: Different electrophoretic mobilities allow distinction between nicked (relaxed) and supercoiled circular plasmid DNA (**Figure 1**).
        3. Remove the incised ssDNA stretch (between the nick sites) from the plasmid by incubation with a ~10-fold excess of the complementary oligonucleotide (oligonucleotide 1 in **Table 1**), shaking at 300 rpm for 30 min near the melting temperature of the oligonucleotide (here: 68 °C for pUC19N) in a heat block (**Figure 1**).
        4. Separate the gapped plasmid from the smaller DNA fragments using a 50 kDa molecular weight cut off (MWCO) filter by centrifugation for 10 min at 10,000 x g in a table centrifuge (**Figure 1**). To extract the concentrated DNA from the filter, invert the filter and insert into a new 1.5 mL reaction tube. Centrifuge for 3 min at 1,000 x g.
        5. Refill the resulting concentrated DNA sample to 500 µL with deionized, filtered water, add an additional ~5-fold excess of complementary oligonucleotide and repeat steps 1.1.1.3 and 1.1.1.4 at least 3 times.
        6. Test for complete gapping of the DNA by incubation with a suitable restriction enzyme (here: XhoI or BglII) using conditions according to the manufacturer's description. Use diluted (nicked versus gapped) DNA samples (~20 nM). Run an agarose gel electrophoresis to distinguish between linearized plasmid (containing no ssDNA gap) and non-incised DNA (gapped DNA) using the nicked DNA as positive control (include a DNA ladder for reference, **Figure 1**). Wear gloves.

    2. Refilling the gap with modified ssDNA oligonucleotides
        1. Anneal the gapped plasmid *via* incubation with a ~25-fold excess of a 5' phosphorylated oligonucleotide that contains the specific target site(s) of choice, incubating at ~45 °C for 4 h (**Figure 1**). Here, use 48 nt ssDNA containing a lesion, either a fluorescein adducted thymine or a cyclobutane pyrimidine dimer (CPD), and in addition a short (8 nt) non-complementary sequence to produce DNA bubbles (see **Table 1**).
        2. Covalently link the annealed insert to the plasmid by incubation with T4 DNA ligase overnight at room temperature according to the manufacturer's protocol (**Figure 1**). For this reaction, add ATP containing concentrated buffer stock solution to produce suitable buffer conditions for the ligase (*e.g.*, use UvrB reaction buffer: 50 mM Tris-HCl pH 7.5, 10 mM $MgCl_2$, 50 mM KCl, 5 mM DTT, 1 mM ATP).
        3. Test for the insertion of the specific oligonucleotide into the gapped plasmid by digestion of diluted samples with a suitable restriction enzyme (same as in 1.1.1.6) according to the manufacturer's protocol followed by an agarose gel electrophoresis (as in 1.1.1.6, **Figure 1**).

    3. Preparation of linear DNA substrate
        1. Digest the modified plasmid DNA with restriction enzymes (ideally with a single restriction site in the plasmid) using conditions as recommended by the manufacturer (**Figure 1**). This step produces linear fragments containing the inserted modification at a defined position. Here, use SspI and BspQI cutting at positions 613 and 255 bp upstream and downstream of the insert, respectively, resulting in a 916 bp DNA fragment containing the specific lesion site at ~30% of the DNA length.
        NOTE: For AFM imaging experiments as described here, DNA fragments with lengths between ~200 bp and ~2,000 bp are suitable substrates.

2. Isolate the target fragment *via* agarose gel electrophoresis and gel extraction using a commercial kit. Wear gloves for protection.
3. Optionally, cut agarose gel with a scalpel to separate the DNA ladder and diluted sample lanes (first two lanes) from the lanes containing the concentrated DNA to be purified. Only expose the gel part with the first two lanes to UV irradiation by placing only this part of the gel on a UV table.
    1. Cut out the band corresponding to the fragment of choice with a scalpel. Re-unite the two gel parts (off the UV table). Use the position of the excised band from the dilute sample as orientation for the position of the band of the desired DNA substrate. Account for the higher concentration by cutting out slightly broader slices than for the dilute control.
    NOTE: Because here, recognition of UV-lesions was investigated, introduction of additional UV lesions *via* UV irradiation was carefully avoided in the DNA substrate by this approach.

4. Calculate the DNA concentration *c* from the absorption at 260 nm measured by a UV-Vis spectrophotometer using Lambert-Beer's law with a double stranded DNA (dsDNA) average molar extinction coefficient of ϵ_{260nm} ~6,700 M^{-1} cm^{-1} per bp:

$$c = \frac{absorption}{\epsilon 260\text{nm} \; x \; L}$$

where *L* is the path length (measurement chamber length, typically 1 cm).

2. **Expression and purification of proteins**
    1. Recombinantly express UvrB in *E. coli* and purify the protein *via* standard chitin bead affinity[15] and size exclusion chromatography[15] as previously described[16].
    NOTE: The *uvrB* gene from *Bacillus caldotenax* had been cloned into the pTYB1 vector.
    2. Express XPD in *E. coli* and purify the protein *via* standard nickel IDA affinity[15] and size exclusion chromatography[15] followed by anion exchange chromatography[15], as previously described[17].
    NOTE: The gene for *Chaetomium thermophilum Xeroderma pigmentosum* group D protein (XPD) had been cloned into the pBADM11 vector. *C. thermophilum* p44 was a kind gift from Caroline Kisker's laboratory, expressed and purified as described[17].

2. AFM Experiment

1. **Sample preparation**
    1. Optionally, pre-incubate the DNA substrate at 65 °C for 10 min in a heat block to remove potential micro-salt crystals that may have formed during storage in the fridge.
    2. Prepare reaction buffer(s) at a 10-fold concentration (10x buffers).
    NOTE: XPD reaction buffer at 1x concentration contained 20 mM Tris-HCl pH 7.5, 10 mM KCl, 5 mM $MgCl_2$, 1 mM TCEP, 2 mM ATP; 1x UvrB reaction buffer contained 50 mM Tris-HCl pH 7.5, 50 mM KCl, 10 mM $MgCl_2$, 5 mM DTT, and 1 mM ATP.
    3. Pre-incubate proteins at a higher concentration in suitable incubation conditions to enhance complex formation. Pre-dilute a small volume (*e.g.*, 1 µL) of the individual proteins in 1x protein reaction buffer to the desired concentration and mix small volumes (*e.g.*, 1 µL) of the individual protein solutions in a 0.5 mL reaction tube.
        1. Place the tube in a heat block for incubation temperatures higher than room temperature. Choose a concentration ratio depending on the expected complex stoichiometry, either equimolar or corresponding concentrations. Here, incubate 1 µL XPD (20 µM in 1 x XPD reaction buffer) and 1 µL p44 (20 µM in 1x XPD reaction buffer) at 10 µM each for 10 min at 37 °C.

    4. Incubate samples at suitable protein and DNA concentrations in protein reaction buffer in a 0.5 mL reaction tube. Here, use 500 nM UvrB or 1 µM XPD + 1 µM p44 and 100 nM DNA. Pipette small volumes to save material, *e.g.*, 0.25-0.5 µL protein (pre-diluted to a 10-fold incubation concentration) and DNA in a total volume of 2.5-5 µL of 1x protein reaction buffer. Here, incubate for 30 min at 37 °C in a heat block. Spin down in a reaction tube briefly (~1 s) in a table centrifuge to ensure mixing of small volumes.

2. **Sample deposition**
    1. Prepare a mica substrate: cut an approximately 1 x 1 cm^2 piece of mica from larger strips using a scalpel. Strip off top layers of the multi-layered mica mineral piece using adhesive tape to reveal a clean, flat, and atomically smooth substrate surface.
    NOTE: The mica piece can be re-used for multiple experiments by stripping off further layer(s).
    2. Prepare the AFM deposition buffer with deionized, filtered water, *e.g.*, 25 mM HEPES pH 7.5, 25 mM Na-acetate, 10 mM Mg-acetate. Filter through a 0.02 µm syringe filter.
    NOTE: Divalent cations in the deposition buffer serve to chelate the negatively charged DNA molecules to the mica surface, which also is negatively charged at neutral pH. If the relatively high Mg^{2+} ion concentration in the deposition buffer poses a problem for a particular protein-DNA system, alternatively, the mica surface can be pre-loaded with amino groups using silatrane-based chemistry to provide positive surface charges for anchoring[18]. Sample deposition can then be carried out in a buffer that contains no or only low amounts of divalent cations.
    3. Dilute the sample (see 2.1) for immediate deposition onto mica in deposition buffer. Deposit a small volume (here: 20 µL).
    NOTE: Dilution factors depend on the sample concentration. Here, dilute samples 50-100x. As a rule of thumb, ~1 nM DNA results in a good surface coverage for ~1,000 bp.
    4. Immediately rinse sample three to four times with a few milliliters of filtered, deionized water, blot off excess liquid, and blow dry in a gentle stream of nitrogen. The entire process from sample deposition to dried samples can be carried out within less than 30 s.
    5. Fix the piece of mica on a microscope slide using adhesive tape at its edges.
    NOTE: Different AFM systems have different requirements for fixing the sample to the stage. Other AFMs possess magnetic stages, and the mica pieces are fixed onto magnetic disks, *e.g.*, using thermal glue. Details of the AFM system used here can be found in the Table of Materials.

3. **AFM imaging**

1. Place the sample (see 2.2.5) centrally on the AFM stage and fix the microscope slide on the stage with magnetic pads.
2. Insert the AFM tip into the tip holder. Use cantilevers with a sharp (<10 nm) AFM probe suitable for oscillating, intermittent contact mode imaging in air. Use AFM probes, for example, as listed in the **Table of Materials**. Here (depends on AFM), fix the tip in the holder under a clamp by tightening the clamp screw (finger tight). Insert the tip holder into the AFM measurement head. Rest the head on its back for this step.
3. Place the AFM measurement head on top of the sample. Details depend on the AFM model. Here, make sure the head stands stably with its legs inside the stage indentations. Make sure the mica is located on the stage where the AFM tip will hover directly above it. Micrometer screws on the right of the stage allow for fine positioning of the sample.
4. Align the AFM laser on the back of the cantilever for optimal signal strength from the position sensitive photodetector onto which the laser is reflected. Details depend on the AFM model.
    1. Here, turn the wheels at the right side and back of the AFM measurement head to adjust the x- and y-positions of the AFM laser to direct it centrally onto the end of the cantilever. Watch the reflection signal in the AFM video window (if available, here: press the camera icon and chose input: Svideo).
    2. Once crudely positioned, optimize the detector sum signal (Sum in Sum and Deflection Meter window in AFM software) by fine tuning the laser position with the two wheels (stay at the end of the cantilever, the sum signal depends on the AFM and cantilever type, here: aim for sum >5).
5. Zero the difference signal from the top and bottom diodes of the detector array (here: Deflection signal in Sum and Deflection Meter window) by directing the AFM laser reflection onto the detector center (here: turn the wheel at the left side of the AFM measurement head).
   NOTE: Deviations from zero then indicate the deflection of the cantilever due to surface interactions, which are translated into height information by the AFM.
6. Determine the cantilever resonance frequency by a frequency tune implemented into the AFM software (here: command auto tune in Master Panel/Tune window). Choose an amplitude corresponding to 1 V input for the piezo that drives the cantilever oscillation. Set the oscillation frequency to slightly (5%) lower than the resonance frequency and zero the phase of the oscillation.
7. Approach the tip to the sample surface using the crude engage mode (here: command Engage in Master Panel window) until the protective setting (set-point) is reached. Use ~2% cutting of the free level oscillation amplitude as the set-point (here, enter Set Point 980 mV in the Master Panel).
8. Fine-engage the AFM tip with the sample surface by lowering the set point using the AFM software. Aim for repulsive mode imaging with the cantilever oscillation phase (Phase in Sum and Deflection Meter window) just below the free level phase (before engage, here typically ~70). Here, use typical final set points on the order of 70-80% of the free level amplitude (1 V).
9. Before scanning, choose the signals for recording in the Master Channel Panel. Choose height (Ht) and amplitude (Am).
10. Begin sample scanning (here: command Do Scan in Master Panel window). Use a scan speed of e.g., 2.5 µm/s (command Scan Speed in Master Panel) to image surface areas of 4 µm x 4 µm or 8 µm x 8 µm (enter Scan Size in Master Panel) with pixel resolutions of 2,048 or 4,096 (Scan Points and Scan Lines in Master Panel), respectively.
11. Save the image file (command Save Image in Master Panel) with no fitting modifications (choose None in Master Channel Panel/Save Plane Fit).
12. For further analysis, process the saved image. Load the image (command Browse Saved Data in the AFM Analysis menu). Open the Modify Panel (press M in the top section of the image). Apply a planefit in x and y dimensions to the height image (extension HtR) (command XY in Planefit window in Modify Panel, choose Planefit Order 3). Then flatten the image (command Flatten in Flatten window in Modify Panel) choosing Flatten Order 3.
13. Export the image as a TIFF file (press Commands in top section of image, choose TIFF Export 2x corresponding to 2,048 pixel resolution) for further analysis.

3. AFM Analysis

1. **Protein complex volume**
    1. Pre-select relevant protein-DNA complexes by direct visual inspection of the images in the AFM software, using a suitable color scheme to maximize different appearances of different size complexes (see different colors and sizes of different complexes in **Figure 2**; here: color scheme SeaLandAndFire in the AFMsoftware). For XPD samples, possible complexes included *XPD/p44-DNA* as well as *XPD-DNA* and p44-DNA, with distinctly different sizes due to the relatively large, different molecular masses of *XPD* (~95 kDa) and p44 (~40 kDa).
    2. Measure volumes of individual protein peaks on the DNA to verify the complex type. This can be achieved with different image software (here: the section tool of the AFM software).
        1. Measure the height (h) and diameter (d) of the protein peak sections with the section window cursors. Measure the diameter close to the base of the particle section.
        2. Determine the volume (V) of the peaks using simple mathematical models, *e.g.*, using the following formula, which is based on a spherical cap model:
        $$V = \frac{\pi \cdot h}{6} \cdot \left(3 \cdot \left(\frac{d}{2}\right)^2 + h^2\right)$$
    3. Translate measured volumes into an approximate protein molecular mass.
        1. Initially, calibrate the AFM system for volume to molecular weight (MW) conversion using a range of proteins with known molecular weight (here: a total of 12 experiments with between 25 and 851 data points each were conducted on 5 different proteins in monomeric, dimeric, trimeric, or tetrameric states) [4,19,20]. Deposit and image proteins (as described above, in 2.2 and 2.3) and measure their volumes as described above (3.1.2). Plot the volumes over their known molecular weights. The resulting graph will show a linear relationship between V and MW, the equation for which can be obtained by a line fit to the data. For the AFM system used here, the following relationship was obtained [19]:

$$MW = \frac{(V + 5.9)}{1.2}$$

NOTE: This step does not have to be repeated before each measurement, but is only done once. The volume to MW calibration can be applied to images obtained under similar imaging conditions using AFM probes with slightly varying diameters.

2. Based on their measured volumes (3.1.2) and the V-to-MW calibration (3.1.3.1), determine the approximate MW of the protein complexes[20], which provides information on its molecular content. *E.g.*, for XPD/p44 samples, ~50 kDa, ~100 kDa, and ~140 kDa were obtained, consistent with p44-DNA complexes (or peaks caused by mere DNA superstructure), XPD only peaks, and XPD/p44 peaks, respectively.

2. **Protein complex positions on DNA**
   1. Determine the DNA fragment lengths.
      1. Trace the DNA fragments in the AFM images, *e.g.*, with the freehand line function of a suitable image analysis software (see for example Table of Materials) and measure the length of the line.
         NOTE: Exclude DNA aggregates as well as fragments cut off by the image margins.
      2. Bin and plot the DNA lengths from the entire experiment in a histogram, using suitable data analysis and graphing software (*e.g.*, see **Table of Materials**).
      3. Fit the length distributions with a Gaussian curve in the data analysis and graphing software to determine the length of the DNA fragments. In order to know the position of the inserted DNA target site (see 1.1), only include DNA fragments with the correct length within two standard deviations from the center of the Gauss curve ($y = y_0 + z \exp(-2(x-x_c)^2/w^2)$, where z is a norm factor and x_c and w are the center and full maximum half width of the Gaussian) in further analyses.
         NOTE: The DNA length at the center of the Gauss curve must be close to the theoretical length of the DNA fragment (calculated using 0.34 nm/bp). Lengths of up to 10% shorter than the theoretical value are typical and are likely caused by AFM resolution limits.

   2. Determine positions of protein peaks on DNA substrates.
      1. Measure the distance of the protein peaks from the closer DNA fragment end, as described in 3.2.1.1 and divide by the total DNA length to obtain distances in units of fraction of DNA length.
      2. Bin and plot the measured distances in a histogram using a suitable data analysis and graphing software (see *e.g.*, **Figure 3**). As a rule of thumb, choose a bin size that gives approximately $\sqrt{n}$ bins for n data points.
         NOTE: Since DNA ends cannot be distinguished here, plot only to fraction of DNA length 0.5 (center of DNA fragment). Because DNA end binding is not the focus of the study, exclude DNA ends from the analyses by starting to bin the position data slightly after position 0 (*e.g.*, here: binning from a DNA length fraction of 0.02).

   3. Determine the target site specificity from protein complex position distributions.
      1. Fit the maximum (enhanced binding occurrences) in the position distribution with a Gauss curve as in 3.2.1.3 but footed on the height of background binding (see **Figure 3**).
      2. Calculate the specificity *S* for the specific site versus the nonspecific DNA background (protein molecules bound to non-specific DNA sites) with the following formula[21]

$$S = \frac{A_{sp} \cdot N}{A_{nsp}} + 1 = \frac{A_{sp} \cdot N}{y_0 \cdot fraction\ DNA\ length} + 1$$

         A_{sp}: Number of specific complexes (area under the Gaussian curve)
         A_{nsp}: Number of nonspecific complexes (area of the background, *i.e.* (fraction DNA length) x (average background height y_0); the fraction of DNA length covered here is 0.48 for a histogram starting at 0.02 DNA length)
         N: number of possible DNA binding sites (here: N = 914 excluding DNA ends)

3. **DNA bend angles**
   1. Using the angle tool in a suitable image analysis software, measure the angle β between two lines placed centrally along the DNA backbone and centering at the protein peak (see *e.g.*, inset in **Figure 4**). Measure the angles for a statistically relevant number of protein-DNA complexes (>50, ideally >100)[2,3,5].
      NOTE: The DNA bend angle is defined as 180°-β[2,3,5].
   2. Using data analysis and graphing software (see Table of Materials) produce a bend angle distribution histogram by binning the DNA bend angles.
   3. Fit the bend angle distribution with a Gauss curve. If more than one maximum is apparent in the distribution, choose multiple peak Gauss fit. The center(s) of the Gaussian curve(s) give(s) the average bend angle state of the particular species.
   4. If a shift in the bend angle(s) (maxima of Gaussian fit(s)) is apparent for distributions, for instance, of different protein variants or different protein complex species, apply a student t -test to evaluate the significance level of the changes.

Copyright © 2017 Journal of Visualized Experiments

Representative Results

Distinguishing between different complex types based on protein complex volumes

The helicase activity of the prokaryotic NER helicase UvrB is stimulated by DNA binding[22,23]. UvrB requires an unpaired region in the DNA (a DNA bubble) in order to load correctly onto one of the two single ssDNA strands. *In vivo*, this DNA structure is provided by DNA interactions through another protein of the NER cascade; in *in vitro* experiments, the bubble can be artificially introduced into dsDNA fragments in close proximity to a target lesion. Protein-protein interactions also enhance DNA binding by UvrB[9]. However, once UvrB is loaded on DNA, its activity does not appear to depend on protein co-factors[9]. In contrast, the eukaryotic NER helicase XPD requires interaction with the protein p44, which like XPD is part of the multi-subunit transcription factor IIH (TFIIH) complex *in vivo*, for activation of its helicase activity, but this interaction does not affect XPD binding to DNA[17]. XPD alone is expected to load onto DNA at a DNA bubble, but not translocate to the lesion (in the absence of its helicase activating co-factor). XPD without p44 should hence not be able to interact with and identify the lesion when loaded at a distance from the lesion site. Incubations of XPD with p44 in the presence of lesion containing DNA substrate result in a mix of XPD- or XPD/p44-DNA complexes (and possibly a minor species of p44 alone bound to DNA). To separately analyze lesion recognition by XPD/p44 and XPD, these different complex types can be distinguished based on their volumes in AFM images (**Figure 2**)[9], as described in Protocol 3.1 above. AFM systems can be calibrated using a range of proteins with known molecular weight, to reveal a linear relationship between the AFM volume and the approximate molecular mass of a protein (complex)[20], allowing an interpretation of the measured volumes. Binding positions on the DNA could thus be separately determined for helicase inactive monomeric XPD (~95 kDa, consistent with the ~100 nm^3 class 2 species in **Figure 2**) and for helicase active XPD/p44 complexes (~135 kDa, ~150 nm^3 class 3 species), based on their different AFM volumes.

Lesion recognition determination from protein binding positions on DNA

Here, long (916 bp) DNA substrates containing a lesion at ~30% of the DNA length were used. Control over the exact position of the lesion within the DNA substrate allows the distinction between specific (lesion-bound, at ~30% of the DNA length) and nonspecific (lesion search) complexes dependent on their positions on the DNA. Two different lesions were chosen, which are targets of NER; DNA substrates contained either a fluorescein (F) adduct or a cyclobutane pyrimidine dimer (CPD). In addition to the lesion site, the DNA contained an unpaired region (8 nt DNA bubble) that served as loading site for the helicases. This loading site was located at a distance of 26 nt (for the F containing DNA substrates) or 23 nt (for the CPD containing substrates) either 5' or 3' from the lesion (see **Table 1**). Lesion recognition leads to stalled DNA translocation of the helicases UvrB and XPD at the target site, apparent in the AFM protein position distribution on DNA as a peak at the position of the lesion. The lesion and bubble positions in these substrates cannot *per se* be distinguished within the resolution limits of AFM imaging (<10 nm distance). However, the fraction of specific complexes that represents the amount of molecules stalled at the lesion and indicates lesion recognition, depended strongly on whether the lesion was placed 3' or 5' from the bubble (**Figure 3**)[9].

From the fraction of complexes at the specific site (area under the Gaussian fit peak versus area of the nonspecifically bound background), the specificity, S, of UvrB and XPD for the two investigated lesion types was calculated (see Protocol 3.2 above). For UvrB, loading 5' from the lesion position resulted in higher specificities ($S_{B,F5}$ ~200 and $S_{B,CPD5}$ ~400) than loading 3' from the lesion ($S_{B,F3}$ and $S_{B,CPD3}$ ~100) for both lesion types. For XPD, complexes containing only XPD (class 2 in **Figure 2**) and complexes containing XPD as well as the helicase activating co-factor protein p44 (class 3 in **Figure 2**) were distinguished as described in the previous section. Class 2 protein peaks (XPD only, helicase inactive) did not preferentially localize at lesion sites independent of whether they were loaded 5' or 3' and independent of the lesion type (data not shown). In contrast, the position distributions for XPD/p44 (class 3) complexes showed enhanced binding at F lesions for loading 5' from the lesion ($S_{XPD/p44,F5}$ ~300 versus $S_{XPD/p44,F3}$ ~100) but at CPD lesions for loading 3' from the lesion ($S_{XPD/p44,CPD3}$ ~600 versus $S_{XPD/p44,CPD5}$ ~100, **Figure 3**). Because UvrB and XPD are 5'-to-3' helicases, these data provide information on whether complexes are stalled *via* interactions with the lesion within the ssDNA strand that they translocate on (the translocated strand, for loading 5' from the lesion), or within the opposite, non-translocated strand (for loading 3' from the lesion). The concept is schematically shown in **Figure 3**. Interestingly, these data hence indicate that specific recognition occurred preferentially on the translocated strand independent of the type of lesion for UvrB, but on different strands for XPD/p44 dependent on the type of lesion. Bulky F lesions were detected preferentially by XPD on the translocated strand, but the only gently DNA distorting CPD lesions on the opposite, non-translocated strand.

Investigating conformational changes upon lesion identification by XPD

Measuring the bending introduced into DNA at the site of bound complexes from AFM images (see Protocol 3.3 above) can reveal important information on complex conformational changes. DNA bend angles were measured for archaeal XPD[5], which does not require protein co-factor interaction for helicase activity. In these studies, a fluorescein lesion was located directly in the context of a DNA bubble for enhanced protein loading at the lesion, at ~30% of the DNA fragment length. Figure 4 shows Gaussian fits to DNA bend angle distributions obtained for protein complexes at nonspecific (non-damaged) DNA positions and at ~30% of DNA length, consistent with XPD bound at the position of the fluorescein lesion (specific complexes). The data demonstrate a mean bend angle of ~50° for nonspecific complexes versus ~65° for specific complexes. This DNA bend angle shift was dependent on the presence of ATP or ATPγs, indicating that ATP (re-)binding but not hydrolysis was necessary for the conformational rearrangements[5].

Copyright © 2017 Journal of Visualized Experiments

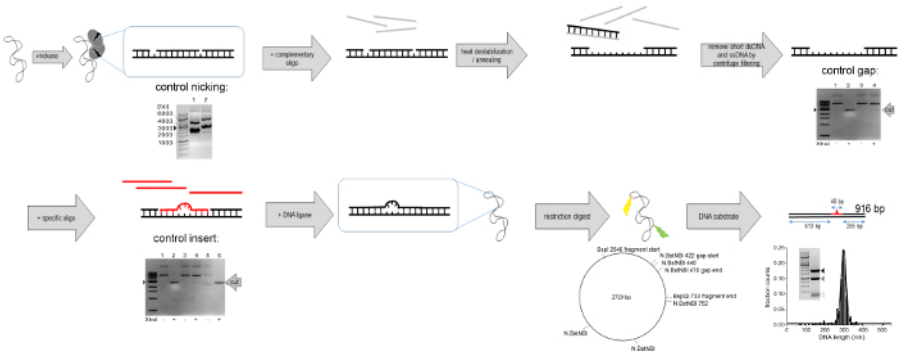

Figure 1: Preparation of DNA substrates. A ssDNA gap is introduced into circular plasmid DNA by nicking the plasmid (here with the nickase N.BstNBI) at closely spaced sites and removing the enclosed ssDNA stretch *via* centrifuge filtration after heat destabilization in the presence of an excess of complementary oligonucleotide. A specific oligonucleotide containing the feature of choice can then be annealed and ligated into the gap region. Finally, digestion with restriction enzymes (here with SspI and BspQI) results in a linear DNA substrate with the target feature at a precisely known position (here at 30% of the DNA fragment length). Control assays allow for testing of the individual steps (shown underneath) *via* agarose gel electrophoresis (black arrow indicates 3000 bp). Nicking can be tested by the altered electrophoretic mobility of the nicked, relaxed circular DNA (control nicking, lane 2) *versus* the supercoiled plasmid (lane 1). Complete gapping of the DNA as well as subsequent insertion of the specific oligo can be tested by digestion with a restriction enzyme that cuts in the gap region (here: XhoI, in lanes 2, 4, and 6) so that a lack of DNA incision indicates gap formation (lanes 1,2 nicked DNA, lanes 3,4 gapped DNA) and re-stalled incision indicates insertion of the specific oligo (lanes 5,6). The final linear substrate that contains the specific feature can be purified from the gel after agarose gel electrophoresis and tested for homogeneity and purity *via* AFM imaging. Please click here to view a larger version of this figure.

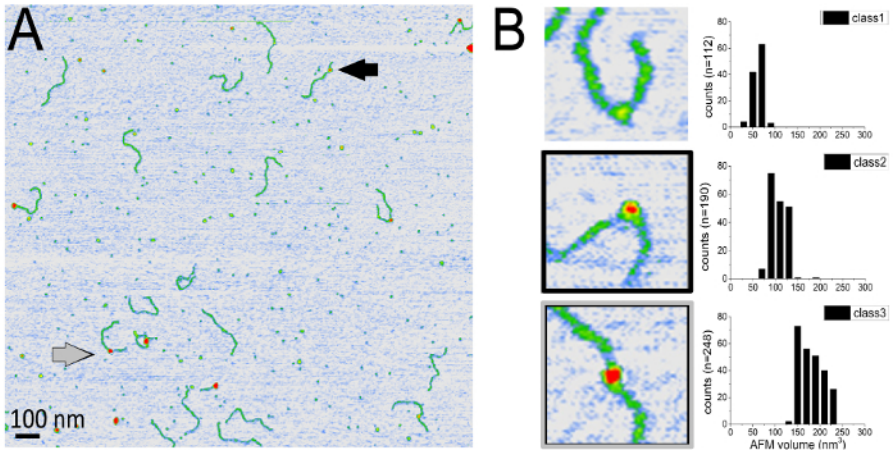

Figure 2: Distinguishing different complex types from their AFM volumes. (**A**) AFM image of XPD/p44-DNA (grey arrow) and XPD-DNA (black arrow) complexes. (**B**) Examples of three different types of DNA bound complexes, interpreted as p44 or mere DNA superstructure (class 1), XPD (class 2, black frame), and XPD/p44 (class 3, grey frame) complexes based on their AFM volumes (shown on the right). Please click here to view a larger version of this figure.

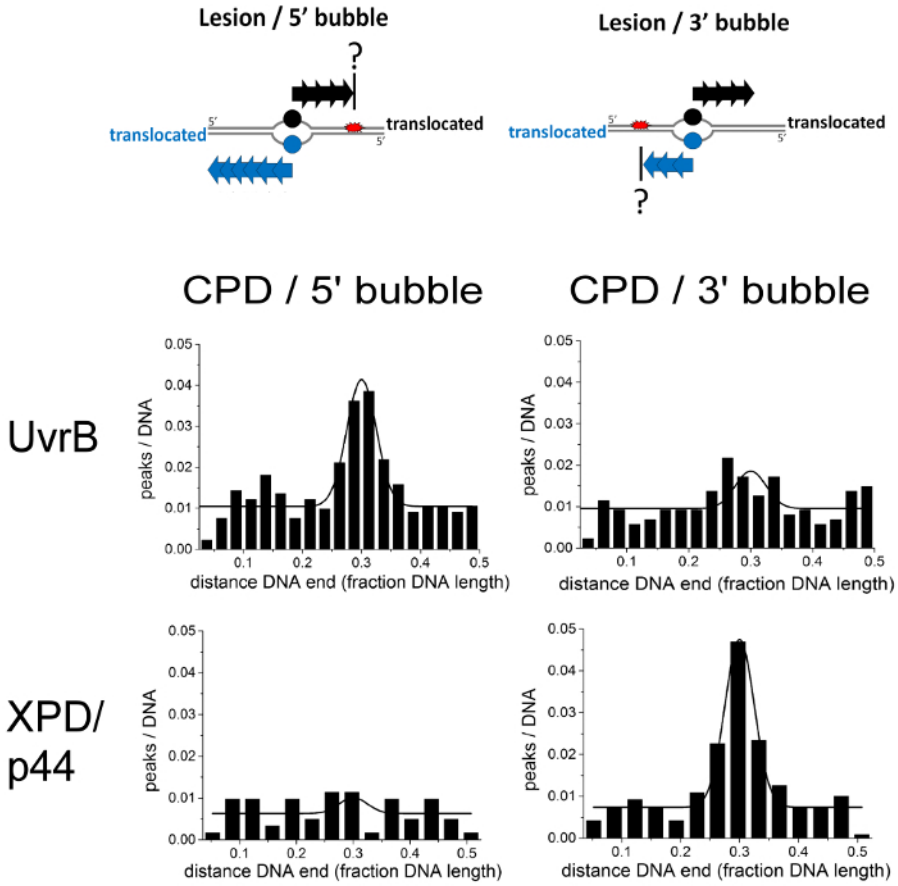

Figure 3: Different lesion recognition strategies of prokaryotic and eukaryotic NER helicases. Lesion recognition competent DNA translocation by the NER helicases UvrB and XPD (in complex with its helicase activating co-factor p44) requires loading of the proteins at an unpaired DNA region (DNA bubble). The proteins then move in 5'-to-3' direction along the ssDNA strand on which they loaded. Recognition of a DNA lesion (here: CPD) by the helicases either on the translocated strand (for loading at 5' bubble) or on the opposite, non-translocated strand (for loading at 3' bubble) results in stalled DNA translocation. In the position distributions this shows as a peak (Gaussian fit lines), which indicates enhanced binding at the lesion position (at ~30% of DNA length for DNA substrates shown here). The prokaryotic NER helicase UvrB and its eukaryotic counterpart XPD show different strategies of CPD lesion recognition that indicate different DNA strand preferences. Specifically, CPD lesions are recognized on the translocated strand by UvrB, but preferentially on the opposite, non-translocated strand by XPD. Figure modified from reference[9]. Please click here to view a larger version of this figure.

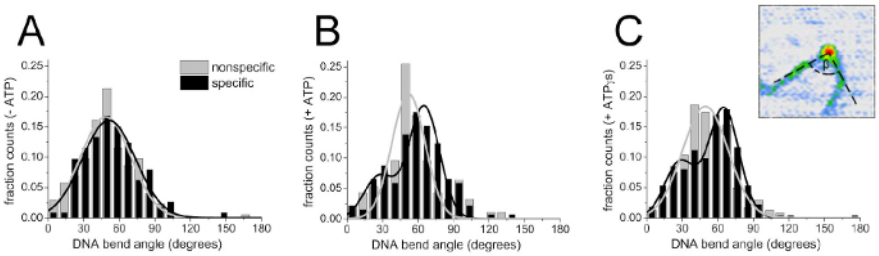

Figure 4: Conformational changes in XPD-DNA complexes upon lesion identification. The distributions of DNA bend angles induced by XPD indicate conformational changes in the protein-DNA complexes at a fluorescein lesion. These conformational rearrangements were dependent on the presence of ATP (B) or ATPγS (C). (**A**) In the absence of ATP, nonspecific bend angles (grey) and bend angles at the lesion site (specific bend angles, black) are similar and fit by a Gaussian curve with center at ~50°. (**B**, **C**) In the presence of ATP or ATPγS, the specific bend angle distribution (black) shows a significant shift ($P = 2.5 \times 10^{-7}$) to an average bend angle of ~65°. This DNA bending at the lesion site was independent of the type of lesion (CPD or fluorescein adduct) or the presence or absence of a DNA bubble[5]. Figure was reproduced from reference[5]. The inset in (C) demonstrates how bend angles (180°-β) were determined. Please click here to view a larger version of this figure.

number	sequence	description
1	GGTCGACTCTAGAGGATCAGATCT GGTACCTCTAGACTCGAGGCATGC	bottom
2	/Phos/GCATGCCTCGTCAAATCTGGT ACCAGATCTGATCCTCTAGAGTCGFCC	F / 5' bubble
3	/Phos/GCAFGCCTCGAGTCTAGAGGT ACCAGATCTCTAAAGTAAGAGTCGACC	F / 3' bubble
4	/Phos/GCATGCCTCGTCAAATCTGGT ACCAGATCTGATCCTCTAGAT-TCGACC	CPD/5'bubble
5	/Phos/GCATGCT-TCGAGTCTAGAGGT ACCAGATCTCTAAAGTAAGAGTCGACC	CPD/3'bubble
6	/Phos/GCA TGCCTCGAGTCTAGACTCF TTCCATCTGATCCTCTAGAGTCGACC	F / bubble

Table 1: DNA oligonucleotides for DNA substrate preparation. All oligonucleotides are 48 nt long and top strands (oligonucleotides 2-6) were obtained phosphorylated at their 5' end for ligation into the gapped DNA (see Protocol 1.1). F = fluorescein adducted thymine, T-T = cyclobutane pyrimidine (thymine) dimer (CPD), non-complementary regions (DNA bubble forming regions) are underlined. F containing oligonucleotides were obtained from Integrated DNA Technologies (IDT), CPD containing oligonucleotides were kindly provided by Thomas Carell's laboratory (Ludwig-Maximilian University Munich, Germany).

Discussion

AFM statistical analyses of binding positions of proteins on long DNA fragments that contain specific target sites can reveal interesting details on the particular strategies employed by the protein to recognize these sites[2,3,4,5,6]. To interpret the resulting position distributions, the positions of the targets in the DNA need to be precisely known. This is achieved by introducing specific sites at well-defined sequence positions into circular plasmid DNA and cutting out a fragment of the DNA including this specific site, using restriction enzyme technology. In AFM image analyses of protein binding positions, only DNA fragments with correct lengths (consistent with the full length of the cut out fragment) can be included because only for these, the position of the target site is known. It is worth noting that the preparation procedure described here results in linear DNA substrates with two indistinguishable fragment ends. Position distributions can hence only be measured and plotted from 0 x DNA length (proteins bound at DNA fragment ends) to 0.5 x DNA length (proteins bound at the center of fragments). Furthermore, for target positions that are not located exactly at the center of the substrate, these distributions always contain a small background of proteins that are nonspecifically bound at the same distance from the other DNA end. However, fitting a Gaussian curve to the distribution footed on the average background height (nonspecifically bound proteins, **Figure 3**) accounts for these complexes. Alternatively, one of the DNA ends can be labeled, for example with small volume peaks from secondary structure forming ssDNA overhangs[24]. Typical resolution limits of these position analyses are in the range of 100-fold preference of target site over nonspecific site binding. In addition, DNA fragment ends do not constitute nonspecific dsDNA sites but instead represent dsDNA breaks. DNA repair proteins often bind to these destabilized fragment ends, in addition to the strand-internally introduced specific target sites. DNA end binding can be revealed by AFM analyses and can provide important information on the function of a protein. If DNA end binding is not the focus of interest, these positions can, however, be easily omitted from the position distributions by starting the plots at a position >0 (*e.g.*, here 0.02 DNA lengths).

One of the particular advantages and, in fact, the defining, common property of single molecule techniques is the resolution of individual, different states present in a sample, which can possess vastly differing properties and activities. Even in cases where the particular species of interest may only be infrequent in a sample, these approaches thus allow the separate focus on this species whose contributions would be dwarfed in an ensemble measurement. For protein samples, for instance, AFM imaging allows the direct distinction between different types of protein complexes based on complex volume, if the sizes of the individual proteins differ sufficiently (typical resolution limits are around 20 kDa)[1,4,6,7,9,12]. AFM systems can be calibrated to allow the translation of the measured volumes into protein molecular weight (Protocol 3.1.3.1)[4,8,19,20]. Alternatively, protein standards with known sizes have been used as a direct reference in the images[1,6]. In the system focused on here, binding positions on DNA could thus separately be determined for the helicase inactive monomeric XPD and for helicase active heterodimeric XPD/p44 complexes. Preferential binding to a lesion site at a well-defined position in the DNA indicated DNA lesion recognition by a protein complex. Since protein loading and lesion sites were spatially separated, DNA translocation was a necessary pre-requisite for lesion recognition in the DNA substrates used here. Only the heterodimeric XPD/p44 complexes were capable of DNA translocation (**Figure 3**), consistent with results from helicase activity assays[9]. AFM volume analysis can hence provide important information on differential activities of different protein complex forms.

Lesion interaction and recognition by the helicase active XPD/p44 complex resulted in enhanced binding at the target site due to stalling of helicase translocation (**Figure 3**). Interestingly, varying the position of the loading site relative to the lesion position resulted in lesion recognition by XPD predominantly when loading occurred 5' from the lesion for bulky fluorescein adducts, but when loading occurred 3' from the lesion for the only little DNA distorting CPD lesion. Because of the 5'-to-3' directionality of XPD helicase (see schematic in **Figure 3**), this finding indicates that the enzyme detects fluorescein preferentially on the translocated strand but CPD preferentially on the opposite, non-translocated strand. The prokaryotic NER helicase UvrB, in contrast, preferentially recognized both fluorescein and CPD lesions upon loading 5' from the lesion, *i.e.* on the translocated strand (**Figure 3**). These distinctive differences in their lesion recognition properties can be understood from the different structural properties of the two helicases. UvrB interacts with potential targets in the DNA *via* amino acid residues on the inside of a β-hairpin feature in the enzyme behind which the translocated strand is likely threaded[16,25]. XPD, on the other hand, hosts a small pore in close proximity to an iron-sulfur (FeS) cluster[26]. The translocated DNA strand likely threads through this pore[26]. Bulkier lesions such as fluorescein may stall helicase translocation *via* interactions with residues within this pore, while less bulky CPD lesions may be identified more easily *via* interactions with the FeS cluster. In the prokaryotic system, two molecules of UvrB are believed to be involved in target site search in a hetero-tetrameric

$UvrA_2$-$UvrB_2$ complex, in which each of the two UvrB monomers is able to investigate a different DNA strand[27]. XPD in eukaryotic NER likely exists as a single copy in the TFIIH lesion recognition complex. Flexibility in lesion interaction approaches of the eukaryotic enzyme may hence be required to enable recognition of the extremely large target site spectrum of the NER repair system.

Because specific (target site bound) and nonspecific complexes can be distinguished in AFM images based on their positions on the DNA, these different complex types can be analyzed separately and compared. Single molecule AFM is one of very few approaches that provide access to structural properties of protein complexes bound nonspecifically to DNA due to their often transient or variable nature. Here, conformational changes upon target site recognition were visualized and characterized in archaeal XPD based on the bending introduced in the DNA by the enzyme. The AFM data revealed a small but distinct, significant shift in DNA bend angles for XPD bound at a lesion site versus XPD bound to nonspecific DNA[5]. Conformational changes in the DNA bound proteins upon target site identification likely trigger the recruitment of the NER endonucleases (XPG and XPF in eukaryotic NER) that carry out excision of a short stretch of ssDNA containing the lesion. Interestingly, this shift and hence conformational re-arrangement required binding of ATP to the enzyme (but not hydrolysis). A similar approach of ATP-rebinding upon target site identification and subsequent recruitment of UvrC endonuclease has been reported for UvrB in prokaryotic NER[28,29].

In summary, AFM single molecule imaging has revealed subtle differences in target site recognition by the prokaryotic and eukaryotic NER helicases. Once a target lesion has been identified by the enzymes, they share a similar strategy of recruiting the NER endonucleases *via* ATP-binding induced conformational re-arrangements selectively at the lesion. The technique of AFM in combination with careful DNA substrate design to mimic essential properties of the investigated system can hence provide insight into target site interactions of not only DNA repair but DNA binding protein systems in general. Structural information on both specific and nonspecific complexes with resolutions in the low nanometer range (at the molecular level, limited by the AFM probe) can contribute significantly to the understanding of the involved mechanisms.

Disclosures

The authors have nothing to disclose.

Acknowledgements

PUC19N, CPD-containing oligonucleotides, and p44 were kindly provided by Samuel Wilson, Korbinian Heil and Thomas Carell, and Gudrun Michels and Caroline Kisker, respectively. This work was supported by grants from the Deutsche Forschungsgemeinschaft (DFG) FZ82 and TE-671/4 to IT.

References

1. Janicijevic, A., Ristic, D., Wyman, C., The molecular machines of DNA repair: scanning force microscopy analysis of their architecture. *J. Microsc.* **212** (3), 264-272 (2003).
2. Wang, H., *et al.* DNA bending and unbending by MutS govern mismatch recognition and specificity. *Proc. Natl. Acad. Sci. USA.* **100** (25), 14822-14827 (2003).
3. Tessmer, I., *et al.* Mechanism of MutS searching for DNA mismatches and signaling repair. *J. Biol. Chem.* **283** (52), 36646-36654 (2008).
4. Wagner, K., Moolenaar, G., van Noort, J., Goosen, N., Single-molecule analysis reveals two separate DNA-binding domains in the *Escherichia coli* UvrA dimer. *Nucleic Acids Res.* **37** (6), 1962-1972 (2009).
5. Buechner, C.N., *et al.* Strand-specific recognition of DNA damages by XPD provides insights into nucleotide excision repair substrate versatility. *J Biol. Chem.* **289** (6), 3613-3624 (2014).
6. Van der Linden, E., Sanchez, H., Kinoshita, E., Kanaar, R., Wyman, C., RAD50 and NBS form a stable complex functional in DNA binding and tethering. *Nucleic Acids Res.* **37** (5), 1580-1588 (2009).
7. Fuentes-Perez, M.E., Dillingham, M., Moreno-Herrero, F., AFM volumetric methods for the characterization of proteins and nucleic acids. *Methods.* **60**, 113-121 (2013).
8. Shlyakhtenko, L.S., Lushnikov, A.Y., Miyagi, A., Lyubchenko, Y.L. Specificity of binding of single-stranded DNA-binding protein to its target. *Biochemistry.* **51**, 1500-1509 (2012).
9. Wirth, N., *et al.* Conservation and Divergence in Nucleotide Excision Repair Lesion Recognition. *J. Biol. Chem.* **291** (36), 18932-18946 (2016).
10. Kuper, J. and Kisker, C. Damage recognition in nucleotide excision DNA repair. *Curr. Opin. Struct. Biol.* **22**, 88-93 (2012).
11. Buechner, C.N. and Tessmer, I. DNA substrate preparation for atomic force microscopy studies of protein-DNA interactions. *J. Mol. Recognit.* **26** (12), 605-617 (2013).
12. Sun, Z., Tan, H.Y., Bianco, P.R., Lyubchenko, Y.L. Remodeling of RecG Helicase at the DNA Replication Fork by SSB Protein. *Sci. Rep.* **5**, 9625 (2015).
13. Billingsley, D.J., Bonass, W.A., Crampton, N., Kirkham, J., Thomson, N.H. Single-molecule studies of DNA transcription using atomic force microscopy. *Phys. Biol.* **9** (2), 021001 (2012).
14. Maurer, S., Fritz, J., Muskhelishvili, G., Travers, A. RNA polymerase and an activator form discrete subcomplexes in a transcription initiation complex. *EMBO J.* **25** (16), 3784-3790 (2006).
15. Green, M.R. and Sambrook, J. *Molecular Cloning: A Laboratory Manual, Volume 1 fourth edition.* Cold Spring Harbor Laboratory Press, Cold Spring Harbor, NY (2012).
16. Theis, K., Chen, P.J., Skorvaga, M., Van Houten, B., Kisker, C. Crystal structure of UvrB, a DNA helicase adapted for nucleotide excision repair. *EMBO J.* **18** (24), 6899-6907 (1999).
17. Kuper, J., *et al.* In TFIIH, XPD helicase is exclusively devoted to DNA repair. *PLoS Biol.* **12** (9), e1001954 (2014).
18. Shlyakhtenko, L.S. *et al.* Silatrane-based surface chemistry for immobilization of DNA, protein-DNA complexes and other biological materials. *Ultramicroscopy* . **97**, 279-287 (2003).

Copyright © 2017 Journal of Visualized Experiments

19. Roth, H.M., *et al.* XPB helicase regulates DNA incision by the Thermoplasma acidophilum endonuclease Bax1. *DNA Repair.* **11** (3), 286-293 (2012).
20. Ratcliff, G.C. and Erie, D.A., A Novel Single-Molecule Study to Determine Protein-Protein Association Constants. *J. Am. Chem. Soc.* **123** (24), 5632-5635 (2001).
21. Yang, Y., Sass, L.E., Du, C., Hsieh, P., Erie, D.A., Determination of protein-DNA binding constants and specificities from statistical analyses of single molecules: MutS-DNA interactions. *Nucleic Acids Res.* **33** (13), 4322-4334 (2005).
22. Caron, P.R. and Grossman, L., Involvement of a cryptic ATPase activity of UvrB and its proteolysis product, UvrB* in DNA repair. *Nucleic Acids Res.* **16** (22), 10891-10902 (1988).
23. Wang, H., *et al.* UvrB domain 4, an autoinhibitory gate for regulation of DNA binding and ATPase activity. *J. Biol. Chem.* **281** (22), 15227-15237 (2006).
24. Chammas, O., Billingsley, D.J., Bonass, W.A., Thomson, N.H., Single-stranded DNA loops as fiducial markers for exploring DNA-protein interactions in single molecule imaging. *Methods.* **60** (2), 122-130 (2013).
25. Truglio, J.J., *et al.* Structural basis for DNA recognition and processing by UvrB. *Nat. Struct. Mol. Biol.* **13** (4), 360-364 (2006).
26. Kuper, J., Wolski, S.C., Michels, G., Kisker, C., Functional and structural studies of the nucleotide excision repair helicase XPD suggest a polarity for DNA translocation. *EMBO J.* **31** (2), 494-502 (2012).
27. Verhoeven, E.E., Wyman, C., Moolenaar, G.F., Goosen, N., The presence of two UvrB subunits in the UvrAB complex ensures damage detection in both DNA strands. *EMBO J.* **21** (15), 4196-4205 (2002).
28. Verhoeven, E.E., Wyman, C., Moolenaar, G.F., Hoeijmakers, J.H., Goosen, N., Architecture of nucleotide excision repair complexes: DNA is wrapped by UvrB before and after damage recognition. *EMBO J.* **20** (3), 601-611 (2001).
29. Moolenaar, G.F., *et al.* The Role of ATP Binding and Hydrolysis by UvrB during Nucleotide Excision Repair. *J. Biol. Chem.* **275**, 8044-8050 (2000).

Copyright © 2017 Journal of Visualized Experiments